Published in final edited form as:
Mol Cell. 2012 December 28; 48(6): 914–925. doi:10.1016/j.molcel.2012.10.011.

VE-cadherin Signaling Induces EB3 Phosphorylation to Suppress Microtubule Growth and Assemble Adherens Junctions

Yulia A. Komarova, **Fei Huang***, **Melissa Geyer***, **Nazila Daneshjou**, **Alexander Garcia**, **Luiza Idalino**, **Barry Kreutz**, **Dolly Mehta**, and **Asrar B. Malik**
Department of Pharmacology and the Center for Lung and Vascular Biology, University of Illinois College of Medicine, Chicago, IL 60612, USA

Summary

Vascular Endothelial (VE)-cadherin homophilic adhesion controls endothelial barrier permeability through assembly of adherens junctions (AJs). We observed that loss of VE-cadherin-mediated adhesion induced the activation of *Src* and phospholipase C (PLC)γ2, which mediated Ca^{2+} release from endoplasmic reticulum (ER) stores resulting in activation of calcineurin (CaN), a Ca^{2+}-dependent phosphatase. Downregulation of CaN activity induced phosphorylation of serine 162 in End Binding (EB) protein 3. This phospho-switch was required to destabilize the EB3 dimer, suppress microtubule (MT) growth, and assemble AJs. The phospho-defective S162A EB3 mutant, in contrast, induced MT growth in confluent endothelial monolayers and disassembled AJs. Thus, VE-cadherin outside-in signaling regulates cytosolic Ca^{2+} homeostasis and EB3 phosphorylation, which are required for assembly of AJs. These results identify a pivotal function of VE-cadherin homophilic interaction in modulating endothelial barrier through the tuning of MT dynamics.

Introduction

The endothelium forms a semi-permeable restrictive barrier that regulates tissue fluid homeostasis and transmigration of blood cells (Komarova and Malik, 2010). VE-cadherin, the main adhesive molecule of AJs, mediates Ca^{2+}-dependent homophilic interaction responsible for adhesion of endothelial cells and formation of a confluent monolayer and endothelial barrier (Vittet et al., 1997). VE-cadherin is a member of a superfamily of glycoproteins possessing a general modular structure of 5 extracellular repeats, a transmembrane domain, and a cytoplasmic tail (Takeichi, 1990). The ectodomains mediate homophilic interaction (Brasch et al., 2011), whereas the cytoplasmic tail interacts with *Armadillo*-repeat gene family proteins (Dejana, 2004) and both kinases and phosphatases (Shasby, 2007) that couple VE-cadherin-mediated adhesion to cell signaling pathways and the actin and MT cytoskeletons (Woodcock et al., 2009). The functions of actin and MTs are critical for the integrity of AJs (Mehta and Malik, 2006; Sehrawat et al., 2008; Sehrawat et al., 2011). A central question in vascular biology is how outside-in signaling emanating

Corresponding Author: Yulia Komarova, ykomarov@uic.edu.
*these authors contributed equally

from VE-cadherin homophilic interaction induces the cytoskeletal changes that regulate endothelial barrier function.

MTs are intrinsically polar filaments with structurally and functionally distinct plus and minus ends (Howard and Hyman, 2003). The minus end is predominantly anchored at the MT organizing center whereas the plus end displays spontaneous growth and shortening (Howard and Hyman, 2009). MT dynamics are finely controlled by plus-end binding accessory factors, which bind to growing MT plus ends (Akhmanova and Hoogenraad, 2005) and regulate the rate of MT growth and shortening as well as the frequency of transitions between these two phases (Akhmanova and Steinmetz, 2008; Howard and Hyman, 2007). The family of EBs represent core elements of a dynamic network at the growing MT plus ends that regulate MT dynamics through recruitment of tubulin-polymerizing and -depolymerizing factors (Akhmanova and Steinmetz, 2008). In cells with a well-defined radial array of MTs, EBs promote persistent MT growth (Komarova et al., 2009) to enable prompt re-organization of MTs and function in concert with the actin cytoskeleton to re-establish the shape of migratory cells (Schober et al., 2009). Here we addressed the question whether VE-cadherin-mediated adhesion influences MT dynamics through modulation of EB protein function and whether these changes in MT dynamics are themselves critical for AJ integrity.

Results

Disruption of VE-cadherin homophilic adhesion induces persistent MT growth

We first examined MT dynamics in primary human pulmonary artery endothelial (HPAE) cells by time-lapse confocal imaging of EB3-YFP and using PlusTipTracker software that enables tracking and analysis of all growing MTs (Applegate et al., 2011; Matov et al., 2010). Based on the deviation from the mean rate and lifetime of growth, the MT population was divided into four groups as indicated in Figure 1 (a, c, e). In confluent endothelial monolayers, MTs grew for a short time (short-lived tracks) with the rate of 17.3±5.5 μm/min and for the mean distance of 4.3±2.3 μm (less than 50% of cell radius) and exhibited frequent catastrophe events in the cell body (Figure 1a–b, Table 1). Disruption of VE-cadherin-mediated adhesion by extracellular Ca^{2+} depletion (see Materials and Methods) or addition of the small inhibitory peptide (SP; RVDAE), which binds to VE-cadherin extracellular 1 module (Heupel et al., 2009) and disrupts VE-cadherin *trans*-interaction (see also Figure S1), increased the number of fast-growing and long-lived (persistently growing) MTs (Figure 1c and e, blue tracks; long-lived MT growth). The length of MT growth from the centrosome increased to 7.4±5.4 μm and 6.8±5.0 μm, respectively, for the above mentioned conditions (Figure 1c–g) and the frequency of catastrophe was also significantly reduced (Table 1). An increase in the number of persistently growing MTs was also evident from the distribution of MT growth tracks (Figure 1d, f) and the greater percentile of long-lived MTs (Figure 1h) in the cells following disruption of VE-cadherin-mediated adhesion. Growth rate was not significantly different between cells with intact and destabilized VE-cadherin-mediated adhesion (Table 1). Thus, these data demonstrate that VE-cadherin-mediated adhesion modulates steady-state MT dynamics by suppressing MT growth.

VE-cadherin-mediated adhesion regulates Ca^{2+} homeostasis through inhibition of *Src*-PLCγ2 signaling

Formation of VE-cadherin adhesion is accompanied by phosphorylation of Tyr^{685} and recruitment of cytosolic C-terminal *Src* kinase (Csk) to AJs (Baumeister et al., 2005; Jin et al., 2010). Csk in turn phosphorylates *Src* at Tyr^{530} to negatively regulate *Src* activity at AJs (Baumeister et al., 2005; Jin et al., 2010). We found that disassembly of VE-cadherin-mediated adhesion induced *Src* activation as indicated by phosphorylation of Tyr^{416} and

decreased phosphorylation of Tyr^{530} (Figure 2a). *Src*-dependent activation of PLCγ is known to result in IP_3 generation (Wang et al., 2009). Using a FRET-based Ins-1,4,5-trisphosphate (IP_3) biosensor, LIBRAvIIS, a high affinity and selectivity probe for IP_3 (Tanimura et al., 2009), we found that destabilization of VE-cadherin-mediated adhesion was accompanied by activation of PLCγ2 and concomitant synthesis of IP_3 (Figure 2b), the intracellular messenger that releases $[Ca^{2+}]i$ from intracellular stores (Mikoshiba, 2007). Knockdown (KD) of PLCγ2 but not PLCγ1 (Figure 2b and S2) significantly altered IP_3 synthesis in cells subjected to Ca^{2+}-free media indicating that VE-cadherin-mediated adhesion provides the spatial cue for inhibition of *Src* and PLCγ2 activities in intact endothelial monolayers. In addition, we observed that disruption of VE-cadherin-mediated adhesion induced sustained increase in cytosolic $[Ca^{2+}]i$ as quantified by Fluor-4 fluorescence (Fig. 2c–d) and Fura340/380 ratiometric imaging (Figure 2e–f). This rise in $[Ca^{2+}]i$ was inhibited by the PLC inhibitor U73122 (Bleasdale et al., 1990) or IP3 receptor antagonist 2-aminoethoxydiphenyl borate (2-APB) (Maruyama et al., 1997) (Figure 2e–f) indicating that rise in $[Ca^{2+}]i$ was secondary to release of Ca^{2+} from ER stores. Consistent with these data, the onset of destabilization of VE-cadherin-mediated adhesion was characterized by a significant decrease in $[Ca^{2+}]ER$ as demonstrated by loss of FRET in Cameleon D1ER, an ER-specific Ca^{2+} biosensor (Figure 2g–h). Thus, these data show that VE-cadherin-mediated adhesion regulates intracellular Ca^{2+} homeostasis by restraining activities of *Src* and PLCγ2 in the resting endothelial monolayer.

VE-cadherin-mediated adhesion induces CaN-dependent EB3 phosphorylation

We next sought to identify the molecular switch responsible for changes in MT dynamics downstream of VE-cadherin-mediated adhesion. We had previously demonstrated that EB1 and EB3 support persistent MT growth by suppressing MT catastrophes (Komarova et al., 2009), and thus we surmised that VE-cadherin-mediated adhesion might induce changes in MT dynamics by regulating EB protein activity, for example, through regulation of the phosphorylation state of EB proteins. Indeed, we observed that EB3 was reversibly phosphorylated on serine residues in confluent monolayers but dephosphorylated following disruption of VE-cadherin-mediated adhesion (Figure 3a). Loss of VE-cadherin-dependent adhesion; however, had no effect on EB3 phosphorylation on threonine residues (Figure S3) or phosphorylation of EB1 (not shown).

To investigate whether the observed changes in EB3 phosphorylation require *Src* and PLC activity, we pretreated HPAECs with *Src* and PLC inhibitors or downregulated PLCγ1 and 2. Inhibition of both *Src* and PLC as well as depletion of PLCγ2 inhibited EB3 dephosphorylation following the loss of VE-cadherin-mediated adhesion (Figure 3b). PLCγ1 KD had only a marginal effect on EB3 phosphorylation, which is most likely the result of its role in regulating basal IP3 production (Figure 2b). These data together indicate that VE-cadherin homophilic adhesion mediates phosphorylation of EB3 through inhibition of the *Src*-PLCγ2 signaling axis.

To define the phosphatase responsible for EB3 dephosphorylation, we focused on CaN, a protein serine-threonine phosphatase known to be regulated by changes in intracellular Ca^{2+} (Klee et al., 1979), as seen after destabilization of VE-cadherin-mediated adhesion (Figure 2c-f). CaN forms a heterodimer consisting of Ca^{2+}-binding subunit B and calmodulin (CaM1)-binding subunit A, and is activated by Ca^{2+} and CaM1 binding (Rusnak and Mertz, 2000). To address whether CaN activity is required for dephosphorylation of EB3, HPAECs were depleted of subunit B (simultaneous depletion of B1 and B2; see Figure S3), or treated with CaN autoinhibitory peptide (Yang and Klee, 2000), or CaN inhibitors cyclosporin A (CsA) and FK506 (tacrolimus); the two latter compounds inhibit CaN activity by forming an immunological complex with cyclophilin and FK506-binding protein, respectively (Huai et al., 2002). We observed that downregulation of CaN or pre-treatment with each CaN

inhibitor in a dose-dependent manner prevented dephosphorylation of EB3 (Figure 3c). Inhibition of CaN activity also prevented the switch in MT dynamics in cells subjected to the extracellular Ca^{2+} depletion protocol (Table 1, see Figure S3), thereby maintaining the steady-state MT dynamics seen in confluent monolayers. These results demonstrate the causal relationship between Ca^{2+} signaling, CaN-dependent dephosphorylation of EB3, and persistent MT growth.

EB3 forms a ternary complex with CaN and CaM1 and undergoes S162 dephosphorylation

To investigate whether EB3 interacts with CaN in cells with destabilized VE-cadherin-mediated adhesion, we performed immunoprecipitation assays. In these experiments, we observed the transient formation of a ternary complex between EB3, CaN, and CaM1 in HPAECs with destabilized VE-cadherin-mediated adhesion (Figure 4a–b). Consistent with the increased level of EB3 phosphorylation, the interaction between EB3 and CaN was greatly reduced in confluent monolayers and at 30 min of reassembly of VE-cadherin-mediated adhesion (Figure 4a–b). To identify the CaN-CaM1-interacting domain of EB3, we used truncated mutants of EB3 (EB3ΔAc and EB3-NL), artificial EB3 dimers in which the EB3-N or EB3-NL fragments are fused to a leucine zipper motif, and EB2/EB3 chimeras (Figure 4c). We found that the calponin homology domain of EB3 was required and sufficient for EB3 interaction with the CaN-CaM1 complex (Figure 4d). Attachment of GFP via a linker sequence to the N-terminus of EB3 (fragment 2) or substitution of the first 29 amino acids for the corresponding residues of EB2 (fragment 7) significantly reduced EB3 binding to CaN-CaM1 (Figure 4d). In contrast, deletion of the coiled-coil domain induced the formation of the ternary complex. EB2 as well as EB1 (not shown) did not interact with CaN-CaM1.

Using phosphoproteomic analysis, we identified the phosphorylation of only S162 in both HEK293 and human dermal microvascular endothelial (HMEC-1) (Ades et al., 1992) cells in the presence of CsA following exogenous expression of Avi-GFP-EB3 (Figure S4). Furthermore, mutation of S162, but not the known EB3 phosphorylation site S176 (Ban et al., 2009), for the non-phosphorylatable alanine abolished phosphorylation of exogenously expressed GFP-tagged EB3 in both HEK293 (Figure 4e) and HMEC-1 (not shown), as demonstrated by our inability to detect EB3-S162A mutant using the phospho-serine antibody. Further, we observed reversible dephosphorylation of EB3 at S162 using a site-specific Ab (Figure 4f; S5a). These results collectively show that disassembly of VE-cadherin-mediated adhesion induces the formation of a complex between EB3 and CaN-CaM1 resulting in the dephosphorylation of EB3 on S162.

To investigate the physiological relevance of EB3 phosphorylation, we determined changes in EB3 phosphorylation in lung vascular endothelium in the context of endotoxemia-induced lung injury (Bachmaier et al., 2007; Lee and Slutsky, 2010). EB3 was basally phosphorylated in lung endothelium and dephosphorylated during endotoxemia-induced lung edema and injury (Figure 4g; S5b). Thus, EB3 undergoes reversible dephosphorylation in lung endothelial cells depending on stability of VE-cadherin adhesion and permeability of the endothelial barrier induced by endotoxin.

EB3 S162A mutant induces persistent MT growth and disrupts AJs

To determine whether EB3 dephosphorylation controls MT dynamics, EB3S162E-GFP and EB3S162A-GFP mutants were transiently expressed in HPAEC confluent monolayers. The phospho-mimetic mutant S162E did not support persistent MT growth in confluent monolayer (Figure 5a, c, e) consistent with the role of EB3 phosphorylation described above (Figure 3). The S162E mutant also did not affect MT growth in endothelial cells following destabilization of VE-cadherin-mediated adhesion (Table 1). In contrast, the phospho-

defective mutant S162A promoted persistent MT growth in confluent monolayer (Figure 5b, d–e; Table 1). These data support the hypothesis that phosphorylation of EB3 on S162 is responsible for inhibiting its anti-catastrophe activity.

To investigate whether phosphorylation of S162 regulates stability of the EB3 dimer (De Groot et al., 2010) and thereby controls persistent MT growth, we determined the $t_{1/2}$ chain exchange for full-length wild type (wt) and phospho-mimetic S162E proteins using FRET-based assay (De Groot et al., 2010). FRET signal generated as a result of chain exchange between YFP- and CFP-tagged dimeric proteins allowed the calculation of $t_{1/2}$ values (Figure 5f); these were 159.5± 12.8, 60.8±15.6, and 83.3± 15.8 min for wt, wt-S162E, and S162E-S162E pairs, respectively. The value for full-length EB3 was significantly different from both E-E and wt-E pairs (p=0.01). These data collectively demonstrate the critical role of EB3 phosphorylation in regulating the stability of EB3 dimers.

We next addressed whether persistent MT growth, induced by EB3 dephosphorylation at S162, influences the stability of VE-cadherin-mediated adhesion itself. We observed that HPAEC monolayers overexpressing EB3S162A-GFP exhibited reduced accumulation of VE-cadherin at AJs (Figure 6a–b) and decreased basal transendothelial electrical resistance, a measure of AJ integrity (Figure 6c–d). Overexpression of EB3S162E-GFP mutants, however, had no affect on AJ integrity (Figure 6a–d). Thus, phosphorylation of S162 destabilizes EB3 dimers and inhibits persistent MT growth, and thereby supports AJ integrity.

Discussion

In this study we demonstrated that VE-cadherin-mediated adhesion through inhibition of *Src*-PLCγ2 signaling and IP3 generation constitutively maintains ambient cytosolic $[Ca^{2+}]i$ and thereby controls steady-state MT dynamics. Formation of VE-cadherin homophilic adhesions induced the phosphorylation of EB3, a member of the most conserved and ubiquitous family of +TIPs, resulting in suppression of persistent MT growth in confluent endothelial monolayers. EBs are known positive regulators of MT growth that polymerize MTs (Busch and Brunner, 2004), inhibit MT pauses and catastrophes (Rogers et al., 2002; Tirnauer et al., 2002), and facilitate MT rescue (Manna et al., 2008; Tirnauer et al., 2002). We have recently described the role of mammalian EB1 and EB3 as key anti-catastrophe factors (Komarova et al., 2009). The anti-catastrophe activity of EBs may be due to recruitment of growth-promoting (Li et al., 2011; van der Vaart et al., 2011) and destabilizing (Montenegro Gouveia et al., 2010; Stout et al., 2011; Tanenbaum et al., 2011) factors at the MT tips, whose activities and accumulation depend on their interaction with EB1 and EB3 (Jaulin and Kreitzer, 2010; Jiang and Akhmanova, 2011; Li et al., 2011). Here we identified a critical role for EB3 phosphorylation as a requisite molecular switch that destabilizes EB3 dimers and suppresses persistent MT growth in endothelial monolayers with intact VE-cadherin-mediated adhesion. In contrast, disruption of VE-cadherin homophilic interaction (hence, of outside-in signaling), as in vascular inflammation (Lee and Slutsky, 2010; London et al., 2010; Vandenbroucke St Amant et al., 2012), induced EB3 dephosphorylation that supported persistent MT growth and mediated disassembly of the AJ barrier.

We identified S162 of EB3 as the phosphorylation site in endothelial cells regulating MT dynamics. S162 is located in the EB3 linker region, which connects the N-terminal calponin homology (CH) domain with the C-terminal dimerization domain of EBs (Akhmanova and Steinmetz, 2008). The CH domain and the linker contain positively-charged sequences required for binding to the MT lattice *in vitro* (Bieling et al., 2007; Hayashi and Ikura, 2003) and in cells (Komarova et al., 2009), and for suppressing MT catastrophe (Komarova et al.,

2009). EB dimerization is also necessary for anti-catastrophe activity (Komarova et al., 2009), and represents an additional mechanism regulating MT dynamics. We demonstrated that S162 phosphorylation destabilized homotypic EB3 dimers and suppressed MT growth. As S162 phosphorylation was detected in multiple tissues (Huttlin et al., 2010), it may represent a general mechanism for EB3 regulation. Interestingly, the phosphorylation of S176 by Aurora kinases during mitosis was also shown to inhibit EB3 interaction with the ubiquitin-protein isopeptide ligase SIAH-1 and regulate EB3 protein stability (Ban et al., 2009). Our finding supports the concept that phosphorylation at a single EB3 site S162 has a fundamental role in determining MT dynamics in cells.

We observed that dephosphorylation of S162 in the absence of VE-cadherin homophilic interaction was mediated by the serine/threonine phosphatase CaN, which requires intracellular Ca^{2+} for its activity (Klee et al., 1979). EB3 formed a ternary complex with CaN and CaM1 following disruption of VE-cadherin-mediated adhesion. Downregulation or inhibition of CaN prevented EB3 dephosphorylation as well as persistent MT growth following destabilization of VE-cadherin-mediated adhesion, indicating an essential role for Ca^{2+} signaling in regulating the anti-catastrophe activity of EB3. We found that destabilization of VE-cadherin-mediated adhesion promoted *Src*–dependent activation of PLCγ2, and thus *Src* acts upstream of EB3 dephosphorylation in mediating persistent MT growth in endothelial cells. Interestingly, EB3, whose expression is elevated during neuronal maturation (Jaworski et al., 2009), controls localization of p140Cap, a regulator of *Src* tyrosine kinase, and modulates actin dynamics in dendrite spines through control of cortactin function (Jaworski et al., 2009). It is possible therefore that EB3 dephosphorylation also provides a positive feedback loop for spatial activation of *Src* at the cell cortex and thereby coordinates re-organization of MT cytoskeleton and actin polymerization in migrating endothelial cells.

VE-cadherin-mediated adhesion in the resting confluent endothelial monolayer functions to restrain *Src* and PLCγ2 activities and maintain low level of cytosolic Ca^{2+}. Our data show that suppression of the cytosolic Ca^{2+} signal is required to maintain endothelial AJ integrity and barrier permeability in the basal state. We observed that expression of the EB3 phospho-defective S162A mutant destabilized VE-cadherin junctions and the AJ barrier consistent with the key role of the cytosolic Ca^{2+} rise in disassembling AJs. Dephosphorylation of EB3 therefore represents a critical pathway regulating MT dynamics downstream of Ca^{2+} signaling. Although we did not address how persistent MT growth disrupts integrity of AJs *per se*, studies in epithelial cells showed that MT dynamics concentrate E-cadherin at the cell-cell contacts by controlling myosin II localization and activity (Stehbens et al., 2006). It is possible that MT cytoskeleton in endothelial cells similarly functions through regulating myosin II activity. Persistent MT growth also results in accumulation of dynamic MTs at the cell cortex (Komarova et al., 2002b); therefore, repetitive targeting of cell-cell adhesion could potentially lead to accelerated VE-cadherin internalization, a key determinant of loss of AJ integrity (London et al., 2010; Vandenbroucke St Amant et al., 2012).

In conclusion, we demonstrated that VE-cadherin adhesion-dependent outside-in signaling homeostatically regulates cytosolic Ca^{2+} concentration and the anti-catastrophe activity of EB3 in a phosphorylation-dependent manner by restraining the activities of *Src* and PLCγ2 (as described in Figure 6e). VE-cadherin disassembly that occurs in vascular inflammatory diseases would be expected to release *Src* and PLCγ2 inhibition and thus increases cytosolic $[Ca^{2+}]i$ to activate CaN-dependent dephosphorylation of EB3 at S162 and thereby promotes MT growth. Persistent MT growth may coordinate actin polymerization and cell shape change, counteract VE-cadherin clustering at AJs, and disrupt the endothelial AJ barrier resulting in vascular leakage. Thus, VE-cadherin outside-in signaling provides both

temporal and spatial control of the MT cytoskeleton required to support the integrity to AJs and normal endothelial barrier function.

Experimental Procedures

A detailed description of the methods can be found in the Supplemental Information accompanying this manuscript.

Protein expression construct, antibodies and reagents

Table S1 lists all constructs, antibodies, reagents and siRNAs sequences. Short (SP, RVDAE) and scrambled (SP control, ADVRE) peptides were synthesized in UIC Research Resources Center. Rabbit polyclonal antibody against non-phosphorylated and phospho-S162 VPQRT(pS*)PTGPKNMQTC peptides were custom made and affinity purified by Absea (China). Specific binding was validated by ELISA and Dot Blot analysis (Figure S5).

Human EB3-GFP has been described elsewhere (Stepanova et al., 2003); EB3 constructs and EB2-EB3 chimeras (Komarova et al., 2009); BirA (Lee et al., 2010) and Cameleon D1ER (Palmer and Tsien, 2006); His-YFP- and His-CFP-EB3 (De Groot et al., 2010); LIBRAvIIS (Tanimura et al., 2009); Avi-pEGFP-C1 vector was a gift from A. Akhmanova (Utrecht University, The Netherlands). EB3 was cloned into Avi-pEGFP-C1 vector using the BamH1 and EcoR1 sites by T4 DNA ligase (New England Biolabs). Single amino acid mutations of full-length human EB3 were introduced with the QuikChange Site-Directed Mutagenesis Kit (Agilent Technologies).

Protein purification, IP, and Western blotting

His-YFP- and His-CFP-EB3 or S162E mutant were purified as described (De Groot et al., 2010) and as detailed in the Supplemental Information. For IP experiments, HPAEC and HMEC-1 were transfected using FuGENE® HD Transfection Reagent (Promega) according to manufacturer's protocols. IP with anti-GFP, -EB3 and CaM1 antibodies and Western blot analysis were performed as described elsewhere (Siddiqui et al., 2011).

Cell culture and treatments

HPAECs (Lonza) were grown in EGM-2 medium (Lonza) and used at passages 2–6. HMEC-1 cells (Ades et al., 1992) were grown in MCDB 131 medium (GIBCO) supplemented with 10% FBS, h-EGF (0.003μg/ml), hydrocortisone (0.001mg/ml) and L-glutamine. HEK 293 cells (ATCC) were grown in DMEM medium (GIBCO) supplemented with 10% FBS. VE-cadherin-mediated adhesion was destabilized by Ca^{2+} switch (10 minutes in Ca^{2+}- and serum-free media) or by incubating with 100μM SP for 1 hour; 100μM SP scrambled peptide was used as a control. Cells were treated with inhibitors as indicated in Table S1 (unless otherwise specified) for 30 minutes.

Phosphoproteomic analysis

EB3 was purified by Avidin-Biotin affinity-based separation as described (Lee et al., 2010). EB3 phosphorylation sites were analyzed as detailed in the Supplemental Information by Taplin Biological Mass Spectrometry Facility (Harvard Medical School).

Analysis of EB3 dimerization

FRET measurements were carried out as described (De Groot et al., 2010) and using a PHERAstar FS (BMG LABTECH Inc., Gary, NC) microplate reader equipped with a FRET module for CFP and YFP. For kinetic measurements, CFP and FRET fluorescence were recorded using simultaneous dual emission at λ=480 and 530 nm, respectively, and

excitation at λ=420nm. FRET was corrected for YFP bleed-through and FRET/CFP ratio was used to calculate $t_{1/2}$. An exponential function was fitted to the data points: B-(B-C)(1-e^(-*k*t)), where B is the basal value, C is the asymptote, *k* is the rate constant and t is time in minutes. $t_{1/2}$ values were calculated from Ln(2)/*k*.

Fluorescent and fluorometric measurement of intracellular free $[Ca^{2+}]_i$

Intracellular free $[Ca^{2+}]_i$ concentration was recorded in a single cell with a fluorescent Ca^{2+} indicator Fluor-4, AM and a ratiometric Ca^{2+}indicator Fura-2 AM as described (Schroder et al., 2011; Stout et al., 2011) and detailed in the Supplemental Information.

Immunofluorescence staining and image analyses

Cell were fixed, stained as described (Komarova et al., 2002a) and imaged as described (Siddiqui et al., 2011) and as detailed in the Supplemental Information. The average fluorescence intensity at AJs and percent of adhesion area was calculated as described (Siddiqui et al., 2011). Relative concentration of IP3 generation and $[Ca^{2+}]_i$ in ER was determined by FRET-based sensor as detailed in the Supplemental Information. All images were processed and analyzed as described (Siddiqui et al., 2011).

Live cell imaging and quantification of MT dynamics

Time-lapse imaging was performed at 37°C using a Nikon Eclipse TE-2000S microscope equipped with UltraView confocal head (PerkinElmer Life Sciences), ORCA-ER-1394 camera (Hamamatsu), AR/KR three line laser (λ=488, 568 and 647 nm), a Plan Apo 100× 1.4 NA objective and Volocity 5 software (Improvision). Images were acquired every 3 seconds. MT growth was analyzed using a PlusTipTracker software package (Matov et al., 2010). Detection, tracking, and post-processing analysis were performed on the 50–100 frames. Tracking control parameters were: 3 minimum and 12 maximum frames for forward and backward gaps; 5–10 pixels as a search radius; 25° and 8° for maximum forward and backward angles, respectively; 1.0 for maximum shrinkage factor; 2 pixels for fluctuation radius as described (Myers et al., 2011).

The ‘Quadrant Scatter Plot’ tool, a part of PlusTipTracker package, was used to determine the relationship between growth rate and growth lifetime and to divide MTs into four sub-populations based on deviation from mean growth speed and growth lifetime (Applegate et al., 2011). The length of MT growth from the centrosome was measured using MetaMorph software based on tracks generated with plusTipTracker and presented as the histogram of length distribution. The catastrophe frequency was calculated from the number of reclassified backward gaps.

Transendothelial monolayer electrical resistance (TER) measurements

TER was determined as described (Garcia et al., 2011). Cells were plated onto gelatin-coated 8W1E gold electrodes (Applied Biophysics) and transfected with EB3 and EB3 mutants. Changes in electrical resistance were monitored starting 30 minutes after transfection using an Electric Cell Substrate Impedance Sensing system (Applied Biophysics Inc.).

Fractionization of pulmonary vascular endothelium

Male CD1 mice received a single dose (10 mg/kg) of LPS intraperitoneally and were used for extraction of endothelial lysates at various times as detailed in the Supplemental Information.

Statistical analysis

Data handling was performed using SigmaPlot software (SPSS, Chicago, IL) and GraphPadPrism (La Jolla, California). Comparisons between groups were made using an ANOVA test and pairwise comparisons were performed using the Tukey post-test method. The changes in the rate of MT growth and catastrophe frequency were compared between experimental and control groups using paired, two-tailed Student *t*-test.

Supplementary Material

Refer to Web version on PubMed Central for supplementary material.

Acknowledgments

We thank Roger Tsien (University of California-San Diego) for the gift of the Cameleon D1ER biosensor; Akihiko Tanimura (University of Hikkaido, Japan) for the gift of the LIBRAvIIS, Michel Steinmetz (Paul Scherrer Institut, Switzerland) for the gift of His-YFP- and His-CFP-EB3, and Anna Akhmanova (Utrecht University, The Netherlands) for providing the pEGFP-Avi-C1 vector. This work was supported by NIH grants R01 HL103922 and Giles F. Filley Memorial Award to Y. K.; R01 HL 45638 to A.B. M.; T32 HL07829-17 support to M. G. and T32 HL07829-18 support to N. D.

References

Ades EW, Candal FJ, Swerlick RA, George VG, Summers S, Bosse DC, Lawley TJ. HMEC-1: establishment of an immortalized human microvascular endothelial cell line. The Journal of investigative dermatology. 1992; 99:683–690. [PubMed: 1361507]

Akhmanova A, Hoogenraad CC. Microtubule plus-end-tracking proteins: mechanisms and functions. Curr Opin Cell Biol. 2005; 17:47–54. [PubMed: 15661518]

Akhmanova A, Steinmetz MO. Tracking the ends: a dynamic protein network controls the fate of microtubule tips. Nat Rev Mol Cell Biol. 2008; 9:309–322. [PubMed: 18322465]

Applegate KT, Besson S, Matov A, Bagonis MH, Jaqaman K, Danuser G. plusTipTracker: Quantitative image analysis software for the measurement of microtubule dynamics. Journal of structural biology. 2011; 176:168–184. [PubMed: 21821130]

Bachmaier K, Toya S, Gao X, Triantafillou T, Garrean S, Park GY, Frey RS, Vogel S, Minshall R, Christman JW, et al. E3 ubiquitin ligase Cblb regulates the acute inflammatory response underlying lung injury. Nat Med. 2007; 13:920–926. [PubMed: 17618294]

Ban R, Matsuzaki H, Akashi T, Sakashita G, Taniguchi H, Park SY, Tanaka H, Furukawa K, Urano T. Mitotic regulation of the stability of microtubule plus-end tracking protein EB3 by ubiquitin ligase SIAH-1 and Aurora mitotic kinases. J Biol Chem. 2009; 284:28367–28381. [PubMed: 19696028]

Baumeister U, Funke R, Ebnet K, Vorschmitt H, Koch S, Vestweber D. Association of Csk to VE-cadherin and inhibition of cell proliferation. EMBO J. 2005; 24:1686–1695. [PubMed: 15861137]

Bieling P, Laan L, Schek H, Munteanu EL, Sandblad L, Dogterom M, Brunner D, Surrey T. Reconstitution of a microtubule plus-end tracking system in vitro. Nature. 2007; 450:1100–1105. [PubMed: 18059460]

Bleasdale JE, Thakur NR, Gremban RS, Bundy GL, Fitzpatrick FA, Smith RJ, Bunting S. Selective inhibition of receptor-coupled phospholipase C-dependent processes in human platelets and polymorphonuclear neutrophils. The Journal of pharmacology and experimental therapeutics. 1990; 255:756–768. [PubMed: 2147038]

Brasch J, Harrison OJ, Ahlsen G, Carnally SM, Henderson RM, Honig B, Shapiro L. Structure and binding mechanism of vascular endothelial cadherin: a divergent classical cadherin. J Mol Biol. 2011; 408:57–73. [PubMed: 21269602]

Busch KE, Brunner D. The microtubule plus end-tracking proteins mal3p and tip1p cooperate for cell-end targeting of interphase microtubules. Curr Biol. 2004; 14:548–559. [PubMed: 15062095]

De Groot CO, Jelesarov I, Damberger FF, Bjelic S, Scharer MA, Bhavesh NS, Grigoriev I, Buey RM, Wuthrich K, Capitani G, et al. Molecular insights into mammalian end-binding protein heterodimerization. J Biol Chem. 2010; 285:5802–5814. [PubMed: 20008324]

Dejana E. Endothelial cell-cell junctions: happy together. Nat Rev Mol Cell Biol. 2004; 5:261–270. [PubMed: 15071551]

Garcia AN, Vogel SM, Komarova YA, Malik AB. Permeability of endothelial barrier: cell culture and in vivo models. Methods Mol Biol. 2011; 763:333–354. [PubMed: 21874463]

Hayashi I, Ikura M. Crystal structure of the amino-terminal microtubule-binding domain of end-binding protein 1 (EB1). J Biol Chem. 2003; 278:36430–36434. [PubMed: 12857735]

Heupel WM, Efthymiadis A, Schlegel N, Muller T, Baumer Y, Baumgartner W, Drenckhahn D, Waschke J. Endothelial barrier stabilization by a cyclic tandem peptide targeting VE-cadherin transinteraction in vitro and in vivo. J Cell Sci. 2009; 122:1616–1625. [PubMed: 19420236]

Howard J, Hyman AA. Dynamics and mechanics of the microtubule plus end. Nature. 2003; 422:753–758. [PubMed: 12700769]

Howard J, Hyman AA. Microtubule polymerases and depolymerases. Curr Opin Cell Biol. 2007; 19:31–35. [PubMed: 17184986]

Howard J, Hyman AA. Growth, fluctuation and switching at microtubule plus ends. Nat Rev Mol Cell Biol. 2009; 10:569–574. [PubMed: 19513082]

Huai Q, Kim HY, Liu Y, Zhao Y, Mondragon A, Liu JO, Ke H. Crystal structure of calcineurin-cyclophilin-cyclosporin shows common but distinct recognition of immunophilin-drug complexes. Proc Natl Acad Sci U S A. 2002; 99:12037–12042. [PubMed: 12218175]

Huttlin EL, Jedrychowski MP, Elias JE, Goswami T, Rad R, Beausoleil SA, Villen J, Haas W, Sowa ME, Gygi SP. A tissue-specific atlas of mouse protein phosphorylation and expression. Cell. 2010; 143:1174–1189. [PubMed: 21183079]

Jaulin F, Kreitzer G. KIF17 stabilizes microtubules and contributes to epithelial morphogenesis by acting at MT plus ends with EB1 and APC. J Cell Biol. 2010; 190:443–460. [PubMed: 20696710]

Jaworski J, Kapitein LC, Gouveia SM, Dortland BR, Wulf PS, Grigoriev I, Camera P, Spangler SA, Di Stefano P, Demmers J, et al. Dynamic microtubules regulate dendritic spine morphology and synaptic plasticity. Neuron. 2009; 61:85–100. [PubMed: 19146815]

Jiang K, Akhmanova A. Microtubule tip-interacting proteins: a view from both ends. Curr Opin Cell Biol. 2011; 23:94–101. [PubMed: 20817499]

Jin H, Garmy-Susini B, Avraamides CJ, Stoletov K, Klemke RL, Varner JA. A PKA-Csk-pp60Src signaling pathway regulates the switch between endothelial cell invasion and cell-cell adhesion during vascular sprouting. Blood. 2010; 116:5773–5783. [PubMed: 20826718]

Klee CB, Crouch TH, Krinks MH. Calcineurin: a calcium- and calmodulin-binding protein of the nervous system. Proc Natl Acad Sci U S A. 1979; 76:6270–6273. [PubMed: 293720]

Komarova Y, De Groot CO, Grigoriev I, Gouveia SM, Munteanu EL, Schober JM, Honnappa S, Buey RM, Hoogenraad CC, Dogterom M, et al. Mammalian end binding proteins control persistent microtubule growth. J Cell Biol. 2009; 184:691–706. [PubMed: 19255245]

Komarova Y, Malik AB. Regulation of endothelial permeability via paracellular and transcellular transport pathways. Annu Rev Physiol. 2010; 72:463–493. [PubMed: 20148685]

Komarova YA, Akhmanova AS, Kojima S, Galjart N, Borisy GG. Cytoplasmic linker proteins promote microtubule rescue in vivo. J Cell Biol. 2002a; 159:589–599. [PubMed: 12446741]

Komarova YA, Vorobjev IA, Borisy GG. Life cycle of MTs: persistent growth in the cell interior, asymmetric transition frequencies and effects of the cell boundary. J Cell Sci. 2002b; 115:3527–3539. [PubMed: 12154083]

Lee HS, Komarova YA, Nadezhdina ES, Anjum R, Peloquin JG, Schober JM, Danciu O, van Haren J, Galjart N, Gygi SP, et al. Phosphorylation controls autoinhibition of cytoplasmic linker protein-170. Mol Biol Cell. 2010; 21:2661–2673. [PubMed: 20519438]

Lee WL, Slutsky AS. Sepsis and endothelial permeability. N Engl J Med. 2010; 363:689–691. [PubMed: 20818861]

Li W, Miki T, Watanabe T, Kakeno M, Sugiyama I, Kaibuchi K, Goshima G. EB1 promotes microtubule dynamics by recruiting Sentin in Drosophila cells. J Cell Biol. 2011; 193:973–983. [PubMed: 21646401]

London NR, Zhu W, Bozza FA, Smith MC, Greif DM, Sorensen LK, Chen L, Kaminoh Y, Chan AC, Passi SF, et al. Targeting Robo4-dependent Slit signaling to survive the cytokine storm in sepsis and influenza. Science translational medicine. 2010; 2:23ra19.

Manna T, Honnappa S, Steinmetz MO, Wilson L. Suppression of microtubule dynamic instability by the +TIP protein EB1 and its modulation by the CAP-Gly domain of p150glued. Biochemistry. 2008; 47:779–786. [PubMed: 18081319]

Maruyama T, Kanaji T, Nakade S, Kanno T, Mikoshiba K. 2APB, 2-aminoethoxydiphenyl borate, a membrane-penetrable modulator of Ins(1,4,5)P3-induced Ca2+ release. J Biochem. 1997; 122:498–505. [PubMed: 9348075]

Matov A, Applegate K, Kumar P, Thoma C, Krek W, Danuser G, Wittmann T. Analysis of microtubule dynamic instability using a plus-end growth marker. Nat Methods. 2010; 7:761–768. [PubMed: 20729842]

Mehta D, Malik AB. Signaling mechanisms regulating endothelial permeability. Physiol Rev. 2006; 86:279–367. [PubMed: 16371600]

Mikoshiba K. IP3 receptor/Ca2+ channel: from discovery to new signaling concepts. Journal of neurochemistry. 2007; 102:1426–1446. [PubMed: 17697045]

Montenegro Gouveia S, Leslie K, Kapitein LC, Buey RM, Grigoriev I, Wagenbach M, Smal I, Meijering E, Hoogenraad CC, Wordeman L, et al. In vitro reconstitution of the functional interplay between MCAK and EB3 at microtubule plus ends. Curr Biol. 2010; 20:1717–1722. [PubMed: 20850319]

Myers KA, Applegate KT, Danuser G, Fischer RS, Waterman CM. Distinct ECM mechanosensing pathways regulate microtubule dynamics to control endothelial cell branching morphogenesis. J Cell Biol. 2011; 192:321–334. [PubMed: 21263030]

Palmer AE, Tsien RY. Measuring calcium signaling using genetically targetable fluorescent indicators. Nat Protoc. 2006; 1:1057–1065. [PubMed: 17406387]

Rogers SL, Rogers GC, Sharp DJ, Vale RD. Drosophila EB1 is important for proper assembly, dynamics, and positioning of the mitotic spindle. J Cell Biol. 2002; 158:873–884. [PubMed: 12213835]

Rusnak F, Mertz P. Calcineurin: form and function. Physiol Rev. 2000; 80:1483–1521. [PubMed: 11015619]

Schober JM, Cain JM, Komarova YA, Borisy GG. Migration and actin protrusion in melanoma cells are regulated by EB1 protein. Cancer Lett. 2009; 284:30–36. [PubMed: 19427113]

Schroder JM, Larsen J, Komarova Y, Akhmanova A, Thorsteinsson RI, Grigoriev I, Manguso R, Christensen ST, Pedersen SF, Geimer S, et al. EB1 and EB3 promote cilia biogenesis by several centrosome-related mechanisms. J Cell Sci. 2011; 124:2539–2551. [PubMed: 21768326]

Sehrawat S, Cullere X, Patel S, Italiano J Jr, Mayadas TN. Role of Epac1, an exchange factor for Rap GTPases, in endothelial microtubule dynamics and barrier function. Mol Biol Cell. 2008; 19:1261–1270. [PubMed: 18172027]

Sehrawat S, Ernandez T, Cullere X, Takahashi M, Ono Y, Komarova Y, Mayadas TN. AKAP9 regulation of microtubule dynamics promotes Epac1-induced endothelial barrier properties. Blood. 2011; 117:708–718. [PubMed: 20952690]

Shasby DM. Cell-cell adhesion in lung endothelium. Am J Physiol Lung Cell Mol Physiol. 2007; 292:L593–607. [PubMed: 17085518]

Siddiqui MR, Komarova YA, Vogel SM, Gao X, Bonini MG, Rajasingh J, Zhao YY, Brovkovych V, Malik AB. Caveolin-1-eNOS signaling promotes p190RhoGAP-A nitration and endothelial permeability. J Cell Biol. 2011; 193:841–850. [PubMed: 21624953]

Stehbens SJ, Paterson AD, Crampton MS, Shewan AM, Ferguson C, Akhmanova A, Parton RG, Yap AS. Dynamic microtubules regulate the local concentration of E-cadherin at cell-cell contacts. J Cell Sci. 2006; 119:1801–1811. [PubMed: 16608875]

Stepanova T, Slemmer J, Hoogenraad CC, Lansbergen G, Dortland B, De Zeeuw CI, Grosveld F, van Cappellen G, Akhmanova A, Galjart N. Visualization of microtubule growth in cultured neurons via the use of EB3-GFP (end-binding protein 3-green fluorescent protein). J Neurosci. 2003; 23:2655–2664. [PubMed: 12684451]

Stout JR, Yount AL, Powers JA, Leblanc C, Ems-McClung SC, Walczak CE. Kif18B interacts with EB1 and controls astral microtubule length during mitosis. Mol Biol Cell. 2011; 22:3070–3080. [PubMed: 21737685]

Takeichi M. Cadherins: a molecular family important in selective cell-cell adhesion. Annu Rev Biochem. 1990; 59:237–252. [PubMed: 2197976]

Tanenbaum ME, Macurek L, van der Vaart B, Galli M, Akhmanova A, Medema RH. A complex of Kif18b and MCAK promotes microtubule depolymerization and is negatively regulated by Aurora kinases. Curr Biol. 2011; 21:1356–1365. [PubMed: 21820309]

Tanimura A, Morita T, Nezu A, Shitara A, Hashimoto N, Tojyo Y. Use of Fluorescence Resonance Energy Transfer-based Biosensors for the Quantitative Analysis of Inositol 1,4,5-Trisphosphate Dynamics in Calcium Oscillations. J Biol Chem. 2009; 284:8910–8917. [PubMed: 19158094]

Tirnauer JS, Grego S, Salmon ED, Mitchison TJ. EB1-microtubule interactions in Xenopus egg extracts: role of EB1 in microtubule stabilization and mechanisms of targeting to microtubules. Mol Biol Cell. 2002; 13:3614–3626. [PubMed: 12388761]

van der Vaart B, Manatschal C, Grigoriev I, Olieric V, Gouveia SM, Bjelic S, Demmers J, Vorobjev I, Hoogenraad CC, Steinmetz MO, et al. SLAIN2 links microtubule plus end-tracking proteins and controls microtubule growth in interphase. J Cell Biol. 2011; 193:1083–1099. [PubMed: 21646404]

Vandenbroucke St Amant E, Tauseef M, Vogel SM, Gao X, Mehta D, Komarova Y, Malik AB. PKCalpha Activation of p120-Catenin Serine 879 Phospho-Switch Disassembles VE-Cadherin Junctions and Disrupts Vascular Integrity. Circ Res. 2012

Vittet D, Buchou T, Schweitzer A, Dejana E, Huber P. Targeted null-mutation in the vascular endothelial-cadherin gene impairs the organization of vascular-like structures in embryoid bodies. Proc Natl Acad Sci U S A. 1997; 94:6273–6278. [PubMed: 9177207]

Wang J, Taba Y, Pang J, Yin G, Yan C, Berk BC. GIT1 mediates VEGF-induced podosome formation in endothelial cells: critical role for PLCgamma. Arterioscler Thromb Vasc Biol. 2009; 29:202–208. [PubMed: 19023093]

Woodcock SA, Rooney C, Liontos M, Connolly Y, Zoumpourlis V, Whetton AD, Gorgoulis VG, Malliri A. SRC-induced disassembly of adherens junctions requires localized phosphorylation and degradation of the rac activator tiam1. Mol Cell. 2009; 33:639–653. [PubMed: 19285946]

Yang SA, Klee CB. Low affinity Ca2+-binding sites of calcineurin B mediate conformational changes in calcineurin A. Biochemistry. 2000; 39:16147–16154. [PubMed: 11123943]

Highlights

- VE-cadherin homophilic adhesion maintains Ca^{2+} homeostasis
- VE-cadherin-mediated adhesion suppresses MT growth
- VE-cadherin-mediated adhesion inhibits CaN-dependent dephosphorylation of EB3
- EB3 phosphorylation is required for suppression of MT growth and formation of AJs

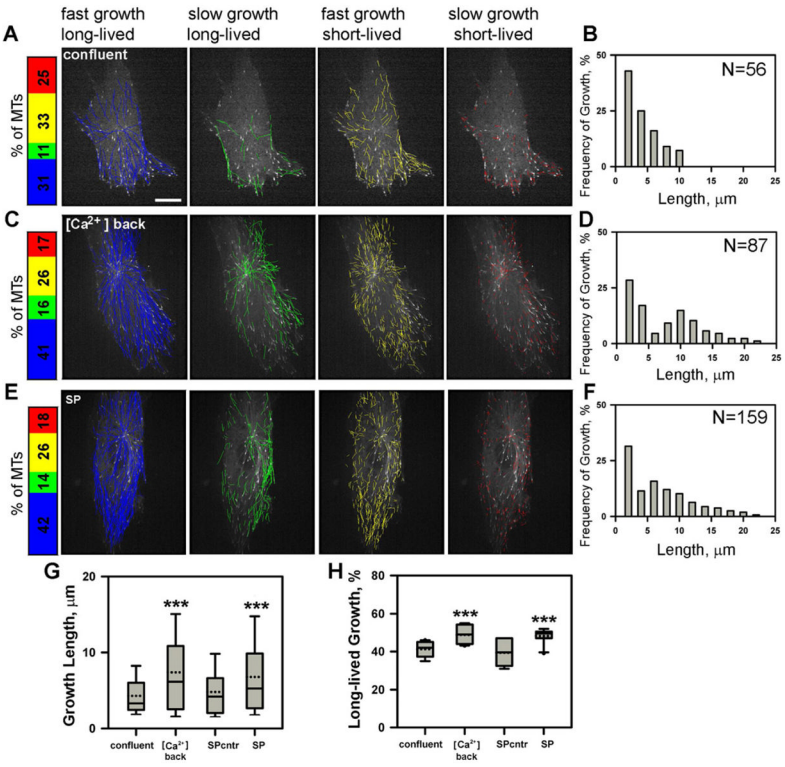

Figure 1. MT growth dynamics in endothelial monolayers with intact or disassembled VE-cadherin-mediated adhesion

(A, C, and **E**) MT growth tracks classified by growth speed and growth lifetime using PlusTipTracker software; (**A**) confluent HPAECs; (**C**) during re-establishing (0–30 min extracellular Ca^{2+} back); or (**E**) destabilization of VE-cadherin-mediated adhesion with anti-VE-cadherin-mediated adhesion peptide that blocks *trans* interaction (see Figure S1). Relative proportions of sub-populations are shown by their corresponding color on left. Disruption of VE-cadherin-mediated adhesion (**C** and **E**) induced fast and persistent MT growth (long-lived MT tracks; blue). Scale bar, 10 μm. (**B, D,** and **F**) Growth length distributions for MTs outgrowing from the cell center for corresponding groups. Increased number of long tracks is consistent with increased number of fast and long-lived MT growth. (**G**) Bar graph of growth length (56, 87, 101 and 159 tracks) and (**H**) percentile of long-lived MT growth (sum of blue and green tracks; n=10 cells per group); mean ± S.D.; **, p=0.005 and ***, p=0.0001.

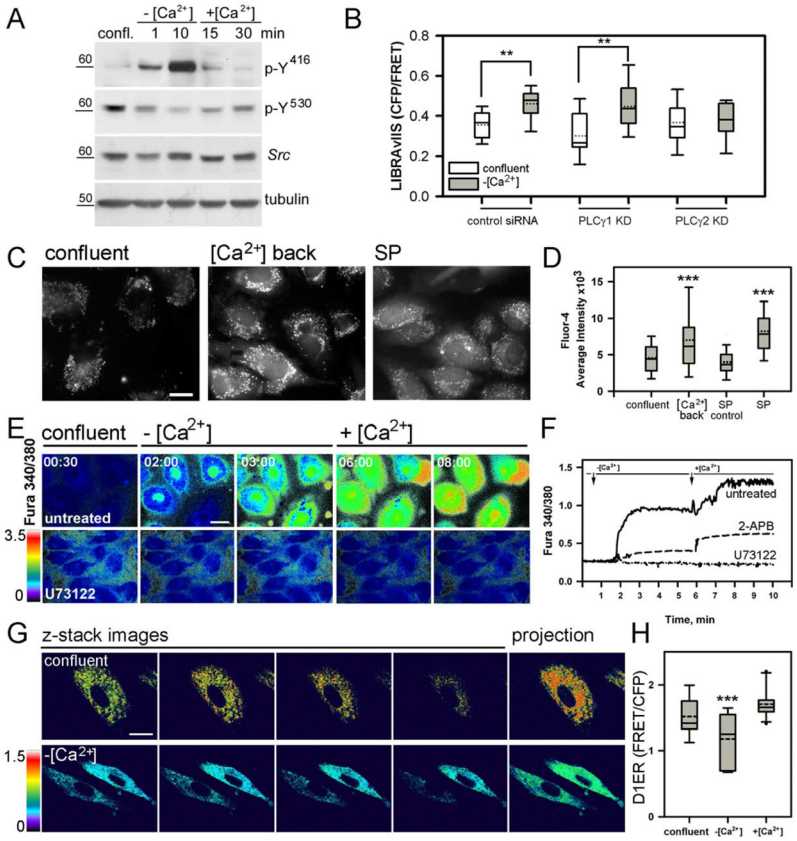

Figure 2. Dissassembly of VE-cadherin-mediated adhesion increases intracellular *[Ca^{2+}]i* via *Src*-PLCγ2 signaling

(**A**) Time-course of *Src* activation during reversible disassembly of VE-cadherin-mediated adhesion in HPAECs by Ca^{2+} switch protocol. −[Ca^{2+}], depletion of extracellular Ca^{2+}; +[Ca^{2+}], Ca^{2+} back. Cell lysates were probed with p-Tyr^{416}, p-Tyr^{530}, and *Src* Abs. Destabilization of VE-cadherin-mediated adhesion increased Tyr^{416} and decreased Tyr^{530} phosphorylation. (**B**) LIBRA vIIS (CFP/FRET ratio) as a measure of IP3 synthesis in HPAECs monolayer with intact (confluent) and destabilized VE-cadherin-mediated adhesion (1 min of Ca^{2+} -free media). PLCγ2 KD inhibited IP3 production as mediated by depletion of extracellular Ca^{2+}; PLCγ1 KD reduced only basal level of IP3. −[Ca $^{2+}$], absence of extracellular Ca^{2+}; n= 10–15 cells/group; mean ± S.D.; ** p=0.002. (**C**) Fluor-4 fluorescence in HPAEC monolayer with intact and destabilized VE-cadherin-mediated adhesion; extracellular Ca^{2+} switch (1–30 min of Ca^{2+} back) or 1 hr treatment with SP or SP control and (**D**) quantification of the data; 102, 114, 132 and 208 cells per group; mean ± S.D.; ***, p=0.0001 *vs.* confluent monolayer and SP control. Scale bar, 10 μm. (**E**) Fura-2AM 340/380 ratiometric images in cells subjected to extracellular Ca^{2+} switch and (**F**) changes in intracellular *[Ca $^{2+}$]i*. Scale bar, 10 μm. Increase in free *[Ca^{2+}]i* was observed after depletion of extracellular Ca^{2+} (−[Ca $^{2+}$]) and as the extracellular Ca^{2+} concentration was increased to 1.5 mM (+[Ca $^{2+}$]). Pretreatment of cells with 2-APB or U73122 significantly reduced the rise in free *[Ca^{2+}]i*. (**G**) *[Ca^{2+}]ER* was measured with Cameleon D1ER (see Methods) in confluent HPAECs, at 2 minute of Ca^{2+} depletion (-[Ca $^{2+}$]) and 15 minutes after Ca^{2+}-add-back (+[Ca $^{2+}$]) and (**H**) quantification of the data. Scale bar, 10 μm. Depletion of extracellular Ca^{2+} reduced *[Ca^{2+}]ER*; n=15 cells/group; mean ± S.D.; ***, p=0.0001.

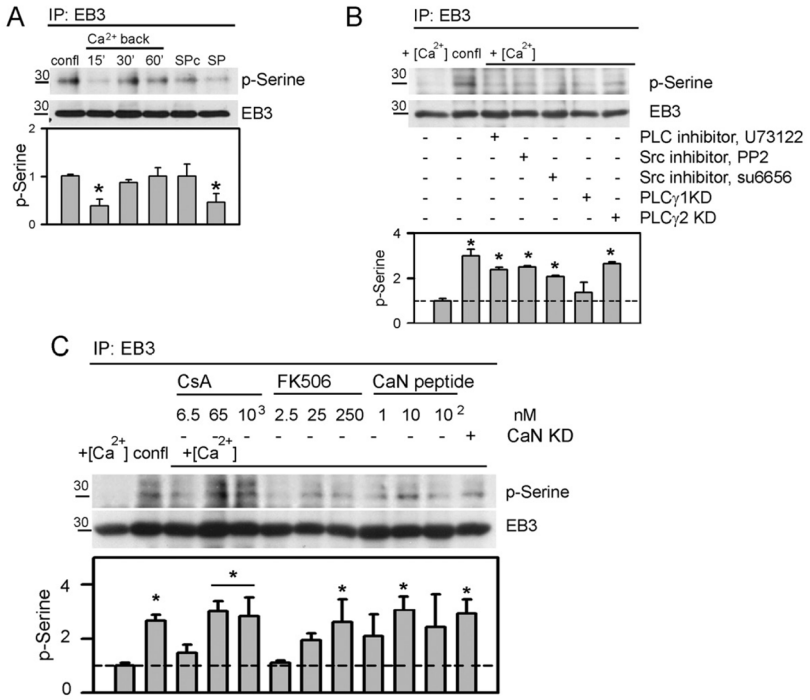

Figure 3. VE-cadherin-mediated adhesion regulates EB3 phosphorylation

(**A**) EB3 undergoes reversible phosphorylation on serine residues. HPAECs underwent Ca^{2+} switch protocol or treatment with SP or SP control peptide for 1 hr. EB3 precipitates probed for phospho-serine and EB3 using Western Blot and quantification are shown; mean ± S.D.; n=4; *, p=0.05. EB3 serine phosphorylation was reduced indicating dephosphorylation following depletion of extracellular Ca^{2+} or SP addition; however, EB3 serine phosphorylation was observed after Ca^{2+}-add-back (at 30 and 60 min) and with control SP. (**B**) EB3 dephosphorylation requires *Src* and PLCγ2 activities. HPAECs were depleted of PLCγ1 and PLCγ2 or treated with indicated inhibitors and subjected to Ca^{2+} switch; after Ca^{2+}-add-back (+[Ca $^{2+}$]) is shown. EB3 phosphorylation was detected as in **A**. Western Blot and quantification are shown; mean ± S.D.; n=3; *, p=0.05. Inhibition of *Src* and PLC activities and PLCγ2 KD inhibited EB3 dephosphorylation following destabilization of VE-cadherin-mediated adhesion. (**C**) EB3 dephosphorylation requires CaN activity. HPAECs were depleted of CaN B1 and B2 (Figure S3) or pretreated with CsA (IC_{50}=65 nM), FK506 (IC_{50}=25 nM), or autoinhibitory peptide (described in Methods) at indicated concentrations and subjected to Ca^{2+} switch protocol. EB3 phosphorylation at 15 min of Ca^{2+}-add-back was determined as in **A**. Western Blot and quantification are shown; mean ± S.D.; n=3; *, p=0.05. Inhibition of CaN induced higher level of EB3 serine phosphorylation.

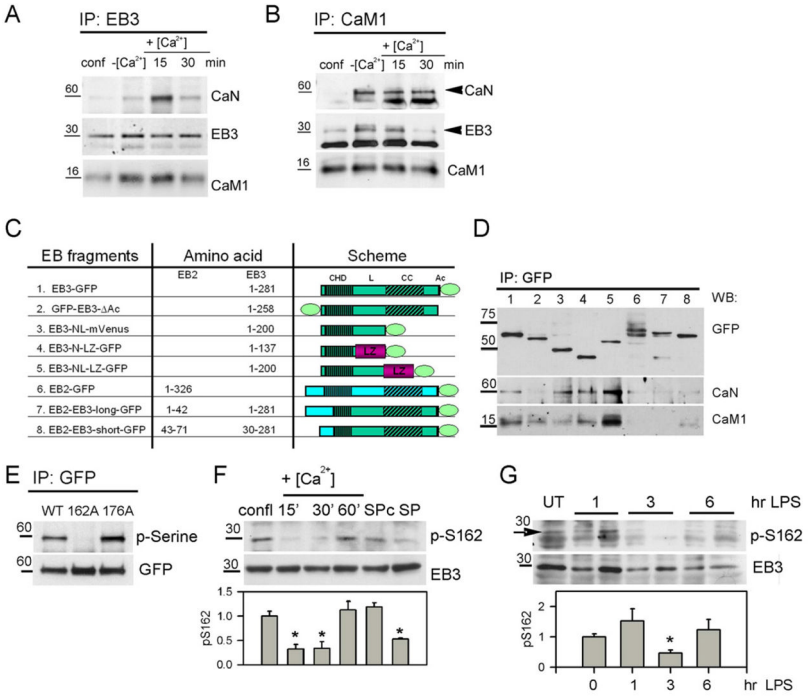

Figure 4. EB3 forms a ternary complex with CaM1 and CaN and undergoes dephosphorylation at S162

(**A–B**) Endogenous EB3 and CaM1 were immunoprecipitated from HPAEC lysates. Resultant precipitates were probed for CaN, EB3, EB1, and CaM1; − [Ca^{2+}], 10 min of Ca^{2+} depletion; +[Ca^{2+}], Ca^{2+}-add-back for indicated times. EB3 formed a complex with CaN and Ca^{2+}-bound CaM1 (16kD); arrowheads indicate CaN and EB3; note, ~25 and 50kD bands are non-specific detection of IgG. (**C**) Representation of EB3 deletion and EB2/EB3 chimera mutants. (**D**) Interaction between EB3-YFP mutants indicated in (**C**) with CaN and CaM1. EB3 mutants were transiently expressed in HMEC-1 and immunoprecipitated with α-GFP Ab and resulting precipitates were probed for CaN and CaM1; EB3 mutants were detected with α-GFP in cell lysate. (**E**) Mutation of S162 abolished EB3 phosphorylation. GFP-EB3 and its mutants, S162A and S176A, were transiently expressed in HEK 293 cells, immunoprecipitated with α-GFP Ab, and resulting precipitates were probed for phospho-serine and GFP. (**F**) EB3 undergoes reversible phosphorylation on S162 residue. HPAEC monolayers were treated as in Figure 3A and cell lysates were probed with phospho-S162-specific Ab and EB3. Western Blot and quantification are shown; mean ± S.D.; n=4; *, p=0.05. (**G**) EB3 undergoes de-phosphorylation on S162 in lung endothelium during inflammation and injury. Mice were given LPS intraperintoneally for indicated times and endothelial-specific lysates from lungs were probed for phospho-S162 and total EB3 using polyclonal rabbit Abs developed in this study; mean ± S.D.; n=4; *, p=0.05.

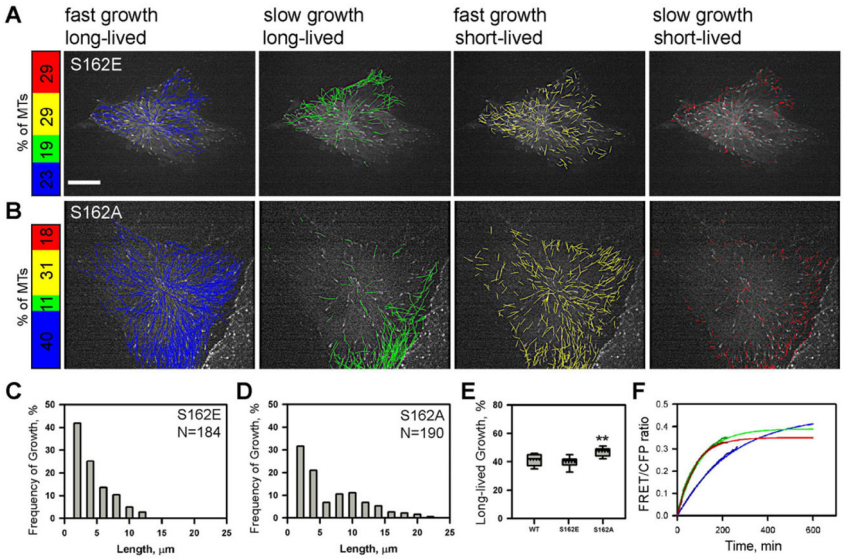

Figure 5. EB3 phosphorylation regulates stability of the dimer and persistent MT growth

(**A–E**) EB3-S162A mutant promotes persistent MT growth in confluent monolayers. Tracks of S162E (**A**) and S162A (**B**) mutants in HPAECs (as in Figure 1). Scale bar, 10 μm. Expression of S162A induced MT growth whereas expression of S162E mutant had no effect. (**C–D**) Growth length distribution for S162E (**C**) and S162A (**D**) tracks outgrowing from the cell center. (**E**) Percentile of long-lived growth (n=10 cells/group); mean ± S.D.; **, p=0.0015. (**F**) The time-dependent increase in FRET after mixing EB3-CFP and EB3-YFP (blue), EB3-S162E-CFP and EB3-S162E-YFP (green), EB3-S162E-CFP and EB3-YFP (red). Average of three experiments (dark) and the best fit are shown (see Material and Methods).

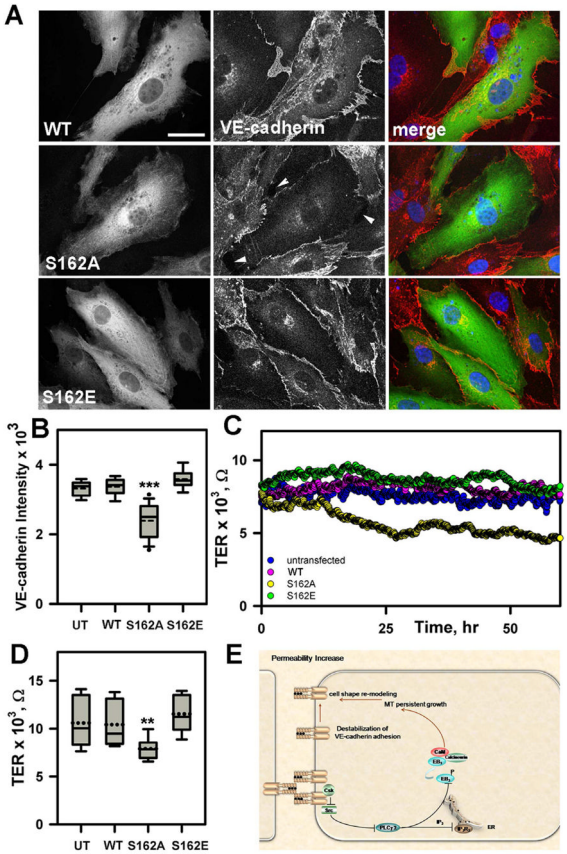

Figure 6. Phospho-defective EB3 S162A mutant decreases VE-cadherin-mediated adhesion and disrupts AJ barrier

(**A**) Immunofluorescent staining of HPAECs expressing EB3, S162A, or S162E mutants. VE-cadherin (red), GFP (green), and nuclei (blue). Bar, 10 μm. Arrowheads show disruption of AJs in cells expressing EB3 S162A. (**B**) Quantification of VE-cadherin expression at AJs; (UT -untransfected cells); n=20 images per group; mean ± S.D.; ***, p=0.0001. Expression of S162A mutant decreased VE-cadherin expression at AJs, which was coupled to opening of AJs (**A**). (**C**) Real-time transendothelial electrical resistance (TER) measurement in HPAECs expressing EB3 or either of the two mutants. Cells grown to 90% confluence were transfected 30 min prior to TER measurements with indicated EB3 plasmids; mean values over time are shown; n= 12. (**D**) Expression of S162A resulted in TER that decreased at 25 hr of transfection. Data are represented as in **B**; **, p=0.0028. Decrease in TER represents a marked disruption of AJ barrier in cells expressing EB3 S162A. (**E**) Model illustrating VE-cadherin outside-in signaling. VE-cadherin homophilic adhesion induces recruitment of Csk to the site of nascent adhesion and inhibits *Src*, downregulates PLCγ2 activity, and induces EB3 phosphorylation. This signaling is translated to non-persistent MT growth, maintenance of cell shape, and stable VE-cadherin-mediated adhesion.

Table 1

Parameters of MT growth.

	Growth Rate [a], μm/min	Catastrophe Frequency [b], min^{-1}
Confluent	17.3 ± 5.5	13.8 ± 3.2
Ca^{2+} back	15.0 ± 5.2	8.4 ± 2. 4 p=0.019
SP control	16.3 ± 4.9	12.3 ± 4.2
SP	18.9 ± 6.4	7.6 ± 3.6 p=0.012; compared SP control
CaN autoinhibitory peptide	14.4 ± 5.1	14.8 ± 8.6 p=0.016
S162A mutant expression; confluent	17.9 ± 6.4	6.1 ± 2.4 p=0.02
S162E mutant expression; confluent	18.7 ± 6.9	10.8 ± 2.3
S162E mutant expression; Ca^{2+} back	17.4 ± 3.7	5.2 ± 3.5 p=0.02
S162E mutant expression; SP	18.0 ± 2.8	4.8 ± 3.4 p=0.009

[a] mean MT growth rate ± S.D.; calculated from the histogram of instantaneous displacement of MT tips between consequent frames;

[b] catastrophe frequency was calculated from the number of reclassified backward gaps (Applegate et al., 2011). Data are presented as mean ± S.D. *p* values were obtained with a paired two-tailed *t*-test with comparison to values in confluent monolayer (except for SP treatment).